Available online at www.sciencedirect.com
SCIENCE DIRECT®
Journal of Nuclear Materials 329–333 (2004) 942–946
journal of nuclear materials
www.elsevier.com/locate/jnucmat

Microstructural evolution in Fe and Fe–Cr model alloys after He^+ ion irradiations

R. Sugano [a,*], K. Morishita [a], A. Kimura [a], H. Iwakiri [b], N. Yoshida [b]

[a] *Institute of Advanced Energy, Kyoto University, Gokasho, Kyoto, Uji 611-0011, Japan*
[b] *Research Institute for Applied Mechanics, Kyushu University, Fukuoka, Kasuga 816-8580, Japan*

Abstract

Thermal desorption spectra (TDS) analysis and transmission electron microscopy (TEM) observation were performed to investigate microstructural evolution in Fe and Fe–X at.% Cr ($X = 5.0$, 15) model alloys during thermal annealing after irradiation with 8 keV He^+ ions at room temperature. TDS analysis showed that there is not so much difference in He desorption during post-irradiation annealing between Fe and Fe–Cr alloys, but the amount of He desorption depended on the Cr concentration of the samples. As for TEM observation, a number of interstitial dislocation loops was observed in all the samples even before post-irradiation annealing, while He bubbles were observed in all the samples only after annealing at temperatures greater than 773 K. Microstructural evolution observed by TEM also depended on Cr concentration. The effect of solute Cr addition on the mobility of interstitial loop and He bubbles is discussed.

1. Introduction

In a first wall material of a fusion reactor, high rates of insoluble He are generated due to nuclear transmutation reaction [1]. It is well known that high He concentrations and formation of He bubbles in metals enhance void swelling and produce high temperature intergranular embrittlement. It is reported that, even considering such He effects, reduced activation martensitic steels (RAMSs) are not inappropriate as a first wall material [2]. This is probably because there are a lot of such potential defects in the steel as dislocations, lath-boundaries, carbides, solute atoms, and so on, which play a significant role for trapping He atoms and preventing He from clustering. For further development of He resistant steels, it is important to clarify the individual roles of the defects on microstructural evolution in metals where He and displacement defects coexist. In our previous paper, the role of dislocations on He trapping in the steel was clarified [3]. In this study, the effects of solute Cr addition on microstructural evolution in Fe and Fe–Cr model alloys irradiated with He^+ ions were investigated using TDS and TEM techniques.

2. Experimental

In the present work, we used the samples of Fe and Fe–X at.% Cr ($X = 5.0$, 15.0) model alloys, where Cr atoms are in a solute state. The ingots of samples were, at first, cold rolled to approximately 0.2 and 0.06 mm thick sheets. Disks with a diameter of 3 mm were punched from the sheet specimens of 0.06 mm thickness for TEM observation, while 0.2 mm thick sheets were cut into 5×10 mm^2 pieces for TDS analysis. All the samples were annealed at 1073 K for 2 h under high vacuum condition (10^{-6} Pa). Then, the samples for TEM observation were electro-polished using a twinjet-polishing unit with an electrolyte solution of 5% $HClO_3$ and 95% C_2H_5OH, while the samples of TDS analysis were electro-polished in a solution of 5% $HClO_3$ and 95% CH_3COOH.

* Corresponding author. Tel.: +81-774 38 3478; fax: +81-774 38 3479.
E-mail address: r-sugano@iae.kyoto-u.ac.jp (R. Sugano).

0022-3115/$ - see front matter © 2004 Elsevier B.V. All rights reserved.
doi:10.1016/j.jnucmat.2004.04.059

All the samples were bombarded at room temperature with the collimated, mass-analyzed beams of monoenergetic He^+ ions. The irradiation dose of incident helium ions was 2×10^{17}, 2×10^{18} and 2×10^{19} He^+/m^2, with the fixed dose rate of about 1×10^{17} $He^+/m^2/s$. The energy of the incident ions was 8 keV, and atomic displacement damage takes place in all the samples. TRIM [4] calculations indicate that this energy corresponds to the approximate helium maximum penetration depth of 100 nm. A displacement damage peak is located at 25 nm from a surface, where the damage rate is 6×10^{-4} dpa/s for 1×10^{17} $He^+/m^2/s$.

TDS analysis and TEM observation were performed to understand the effects of solute Cr addition on microstructural evolution in the samples during post-irradiation annealing after irradiations. In the TDS analysis, the samples were heated up to 1500 K by infrared-ray irradiation with the fixed ramping rate of 1 K/s. During the heating, background vacuum was kept below 10^{-5} Pa and He release was monitored by a quadruple mass analyzer. He atoms retained in the samples were released from surface during the heating. As for the TEM observation, TEM discs were isochronally annealed for 10 min at every 100 K from 573 to 973 K after irradiation. The ramping rate of temperature was fixed at 1 K/s, as same as that used in TDS analysis.

Electron irradiation using HVEM, where atomic displacement damage takes place, was also performed at room temperature and identified the black spot defect as an interstitial type dislocation loop, because the defects grew during the electron irradiation.

3. Results

3.1. He desorption from Fe and Fe–Cr alloys irradiated by He^+ ions

Fig. 1 indicates the Cr concentration dependence of the TDS for the samples irradiated by He^+ ions at room temperature as a function of irradiation dose. In our previous study [5], TDS obtained for Fe showed five different peaks, each of which corresponded to desorption of He atoms dissociated from surface, He_nV ($2\leqslant n\leqslant 6$) and He_nV_m ($1\leqslant n, 2\leqslant m$) and associated with γ-transformation and He bubbles, respectively. The He desorption peaks obtained for Fe–Cr alloys were not so much different from those obtained for Fe, except that there is no He desorption due to γ-transformation in Fe–15Cr [6], where γ-transformation does not take place. It indicates that the solute Cr atom does not produce additional trapping sites for He atoms. However, there is a dependence of Cr concentration on the amount of He desorption observed at each temperature. The amount of He desorption detected at the temperature range from 773 to 973 K decreases with increasing Cr concentration

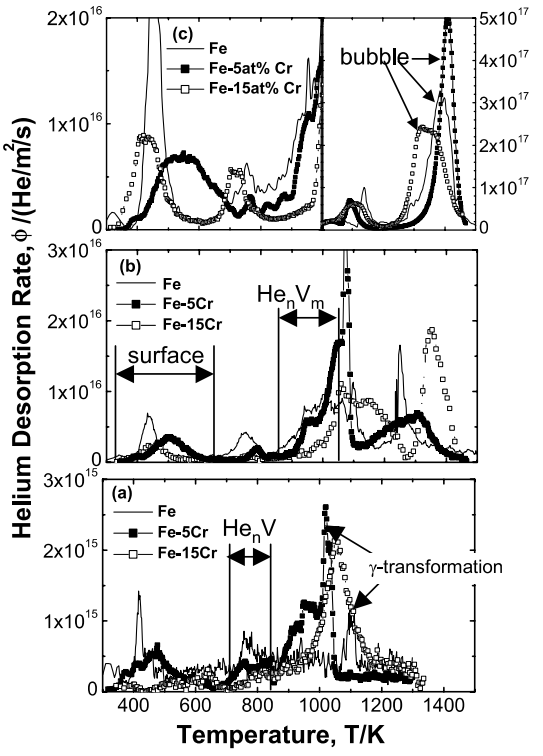

Fig. 1. He desorption spectra of Fe, Fe–5Cr and Fe–15Cr irradiated by 8 keV He+ ions at room temperature. The irradiation doses are (a) 1017, (b) 1018 and (c) 10^{19} He^+/m^2.

for the samples irradiated to 2×10^{18} and 2×10^{19} He^+/m^2, where He desorption associated with He bubbles is observed in the present study.

3.2. TEM micrographs of the dislocation contrast

TEM observations were performed to investigate microstructural evolution in Fe and Fe–Cr alloys during post-irradiation annealing. Fig. 2 shows the microstructures of the samples annealed at 573, 673, 773, 873 and 973 K after the irradiations of 2×10^{19} He^+/m^2. The direction of electron beam is $B=[0\,0\,1]$. A reflection employed here was of $g=110$. As shown on micrographs, black spot defects ranging from 1 to 5 nm in diameter were observed in all the samples.

The areal number density and size of the loops was evaluated by micrographs obtained using the two kinds of reflections, $g=110$ and 200. Since the dislocation loops in Fe have $a\langle1\,0\,0\rangle$ and $(a/2)\langle1\,1\,1\rangle$ components [7], where 'a' is lattice constant, the number density of dislocation loops really existed in the samples can be evaluated with the following equations:

$$\rho_{a\langle1\,0\,0\rangle}=2\rho_{g=110}-\rho_{g=200}, \quad (1)$$

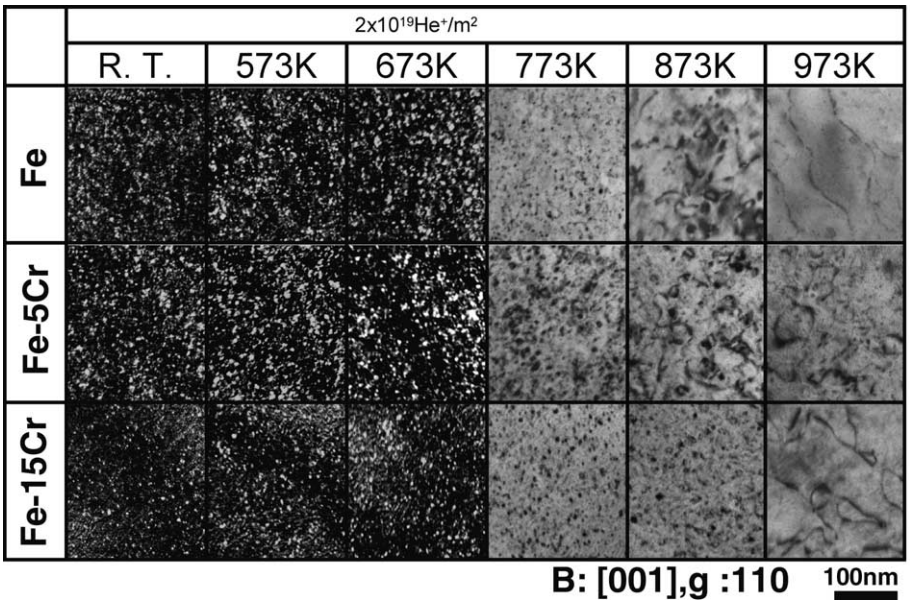

Fig. 2. The microstructural evolution in Fe, Fe–5Cr and Fe–15Cr irradiated by He^+ ions and after post-irradiation annealing at 573, 673, 773, 873 and 973 K.

$$\rho_{(a/2)\langle 1\,1\,1\rangle} = -(2/3)\rho_{g=110} + (4/3)\rho_{g=200}. \quad (2)$$

Here, $\rho_{a\langle 1\,0\,0\rangle}$ and $\rho_{(a/2)\langle 1\,1\,1\rangle}$ is the number density of the loops of $a\langle 1\,0\,0\rangle$ and $(a/2)\langle 1\,1\,1\rangle$ components, respectively, while $\rho_{g=110}$ and $\rho_{g=200}$ is the number density of the loops observed by the reflections of $g = 110$ and 200, respectively. Fig. 3 shows the dependence of Cr concentration on the total number density and average size of the loops, where the total number density is the sum of $\rho_{a\langle 1\,0\,0\rangle}$ and $\rho_{(a/2)\langle 1\,1\,1\rangle}$.

The number density and average size of the loops increased during post-irradiation annealing from room temperature (as-irradiation condition) to 573 K. Such behavior is especially significant for Fe and Fe–15Cr. During annealing from 573 to 673 K, the number density decreased but the size increased, indicating that the migration and growth of interstitial loops took place. When the temperature was increased from 673 to 773 K, there was no significant change in the number density but the size decreased, indicating that the loops were shrunk by vacancies. After annealing at 873 and 973 K, the loops coarsened and changed to line defects in all the samples.

3.3. TEM micrographs of He bubbles

Up to 673 K, He bubbles were not observed in Fe and Fe–Cr alloys during post-irradiation annealing. However, after annealing at 773, 873 and 973 K, high density of bubbles were observed in all the samples as shown in Fig. 4. Fig. 5 shows the size distribution of

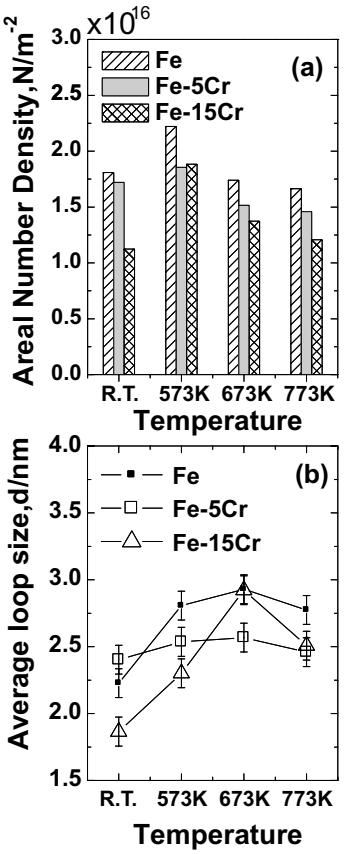

Fig. 3. The chromium concentration dependence of (a) total number density of dislocation loop and (b) average loop size.

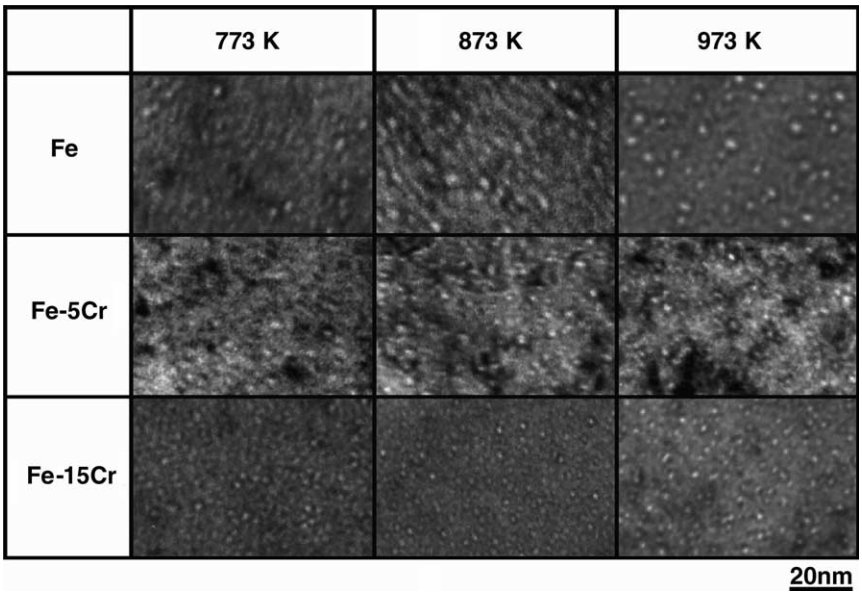

Fig. 4. He bubble microstructure after post-irradiation annealing at 773, 873 and 973 K in Fe, Fe–5Cr and Fe–15Cr.

bubbles observed at 773, 873 and 973 K. When annealing temperature increased from 773 to 873 K, there is no change in the size distributions of bubbles. However, the number density of relatively large-size bubbles increased after annealing at 973 K, resulting in the peak shift of the size distributions to larger range. The peak shift was greater for low Cr alloys.

4. Discussion

4.1. The behavior of interstitial loops during annealing

There are two possible mechanisms to explain an increase in the number density and size of loops during post-irradiation annealing from room temperature to 573 K. One is due to the aggregation of SIAs emitted thermally from the He–V clusters of high He density [8]. The other is the growth by the migration and coalescence of SIA clusters, which were produced by irradiation but were TEM-invisible at room temperature. In the case of Fe, it is considered that there is no invisible small SIA clusters because the mobility of a small SIA cluster is so high [9] that it should migrate freely in the matrix to be annihilated at sinks even at room temperature. Therefore, it is considered that the both the number density and the size were increased by the result of the aggregation of SIAs emitted from He–V clusters during annealing. On the other hand, in the case of Fe–15Cr, since there is no evidence that there are not such invisible clusters, it is not determined here which mechanism is dominant.

The coarsening observed at greater than 873 K may take place by the migration and coalescence of loops in the samples. It seems to depend on Cr addition: namely, the presence of Cr atoms will reduce the mobility of loops.

4.2. The effects of Cr addition on He bubble formation

Recombination between interstitial loops and vacancies observed at annealing temperatures from 673 to 773 K indicates that there are many mobile vacancies in the samples at these temperatures, which are produced due to dissociation from He–V clusters. It is reasonable that such vacancies also contribute to the growth of He–V clusters into He bubbles. In fact, our experimental TEM observation showed that bubbles were first observed at 773 K in all the samples. It is noted here that thermal stability of He–V clusters strongly depends on the He/V ratio in the cluster [8], and in this case, the He–V clusters emitting vacancies have lower He/V ratio while those absorbing vacancies have higher He/V ratio. At higher annealing temperature from 773 to 873 K, the growth of bubbles was not observed in all the samples. This indicates that release and absorption of vacancies from He–V clusters may not take place at the temperatures.

After annealing from 873 to 973 K, the growth of bubbles was observed in the samples as well as significant He desorption. If one considers that the bubble growth in this temperature range is due to the same mechanism mentioned above, i.e., absorption of vacancies,

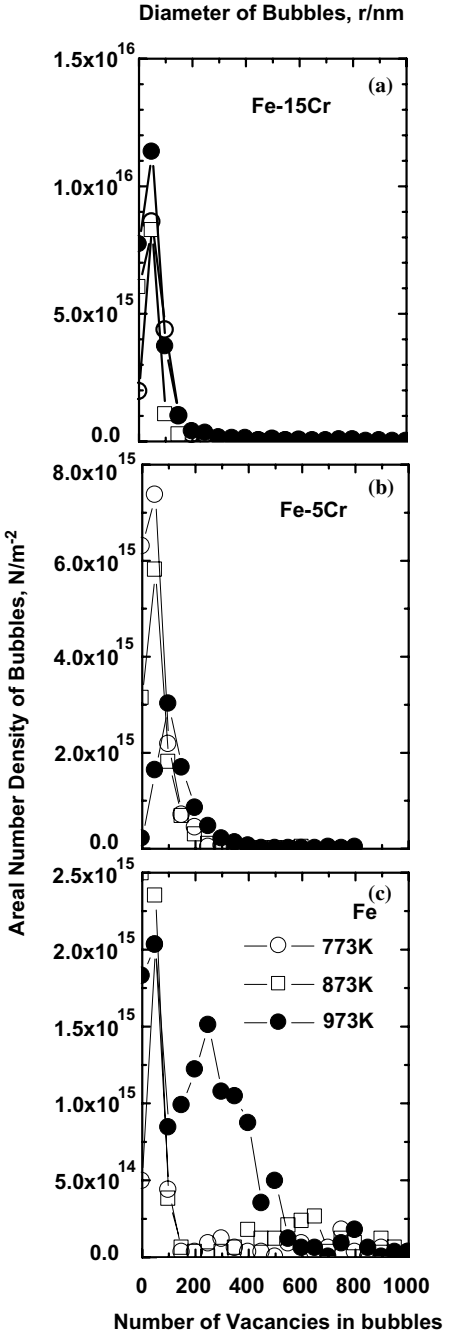

Fig. 5. Size distribution of bubbles observed at 773, 873 and 973 K.

the He–V clusters (including He bubbles) reduce the He/V ratio in the cluster. In this case, such He–V cluster may not emit He atoms any more, because the binding of He to a He–V cluster becomes stronger with the decrease in the He/V ratio in the He–V cluster [8]. This is, however, inconsistent with the fact that significant He desorption was observed. A possible mechanism that can reasonably be considered here is the migration of He–V clusters.

The bubble growth accompanied with significant He desorption observed from 873 to 973 K depends on the Cr concentration of samples. It is more remarkable for less Cr concentration. If the He–V cluster migration mentioned above is the appropriate mechanism, the experiments may indicate that a Cr addition decreases the mobility of He–V clusters. This was reported in the literature [10] in that the diffusivity of TEM-visible bubbles produced by He^+ ion irradiation in Fe–9Cr is lower than that in Fe.

5. Summary

Thermal desorption measurements and TEM observation were performed to investigate microstructural evolution in Fe and Fe–Cr model alloys after He^+ ion irradiations. Cr addition may suppress the migration of interstitial loops and the He–V clusters.

References

[1] B.N. Singh, T. Leffers, J. Nucl. Mater. 125 (1984) 287.
[2] R. Lindau, A. Möslang, D. Preininger, M. Rieth, H.D. Röhrig, J. Nucl. Mater. 271&272 (1999) 450.
[3] R. Sugano, K. Morishita, H. Iwakiri, N. Yoshida, J. Nucl. Mater. 307–311 (2002) 941.
[4] J.P. Biersack, L.G. Haggmark, Nucl. Instrum. and Meth. B 2 (1984) 814.
[5] K. Morishita, R. Sugano, H. Iwakiri, N. Yoshida, A. Kimura, in: Proceedings of the Fourth Pacific Rim International Conference on Advanced Materials and Processing (PRICM-4), J. Jpn. Inst. Met., (2001) p. 1395.
[6] R. Sugano, K. Morishita, A. Kimura, Fus. Sci. Technol. 44 (2003) 446.
[7] J. Marian, B.D. Wirth, R. Schäublin, J.M. Perlado, T. Diaz de la Rubia, J. Nucl. Mater. 307–311 (2002) 871.
[8] K. Morishita, R. Sugano, B.D. Wirth, T. Diaz de la Rubia, J. Nucl. Mater. 323 (2003) 243.
[9] N. Soneda, T. Diaz de la Rubia, Philos. Mag. A 81 (2001) 331.
[10] K. Ono, K. Arakawa, K. Hojou, J. Nucl. Mater. 307–311 (2002) 1507.